Research Article

Advances in Mechanical Engineering

Advances in Mechanical Engineering
2020, Vol. 12(5) 1–11

DOI: 10.1177/1687814020922007
journals.sagepub.com/home/ade
SAGE

A study on the matching of constraint between steam turbine blade and laboratory specimens

Jie Yang[1], Yuman Liu[1] and Haofeng Chen[2]

Abstract

The matching of constraint between laboratory specimens and actual cracked structures is a key problem of the accurate structure integrity assessment. Different laboratory specimens and the steam turbine blade with different constraints were selected, the matching of constraint between steam turbine blade and laboratory specimens was investigated. The results shown that the steam turbine blade with $2c = 50$ mm, $a/2c = 0.20$ has a matching constraint with single edge-notched bend specimen with $a/W = 0.6$ and single edge-notched tensile specimen with $a/W = 0.3$. The steam turbine blade with $2c = 50$ mm, $a/2c = 0.25$ has a matching constraint with single edge-notched bend specimen with $a/W = 0.7$. The steam turbine blade with $2c = 50$ mm, $a/2c = 0.30$ has a matching constraint with single edge-notched bend specimen with $a/W = 0.5$ and single edge-notched tensile specimen with $a/W = 0.1$. The steam turbine blade with $2c = 50$ mm, $a/2c = 0.35$ has a matching constraint with single edge-notched bend specimen with $a/W = 0.4$, compact tension specimen with $a/W = 0.3$ and central-cracked tension specimen with $a/W = 0.7$. The steam turbine blade with $a = 15$ mm, $a/2c = 0.30$ has a matching constraint with compact tension specimen with $a/W = 0.7$ and single edge-notched tensile specimen with $a/W = 0.5$. The steam turbine blade with $a = 15$ mm, $a/2c = 0.40$ has a matching constraint with compact tension specimen with $a/W = 0.4$. The steam turbine blade with $a = 15$ mm, $a/2c = 0.50$ has a matching constraint with single edge-notched bend specimen with $a/W = 0.5$.

Keywords

Constraint, matching, steam turbine blade, laboratory specimen, structure integrity assessment

Date received: 30 October 2019; accepted: 19 March 2020

Handling Editor: Jose Ramon Serrano

Introduction

Constraint is the resistance of a structure against plastic deformation.[1] It was divided into out-of-plane constraint and in-plane constraint. The out-of-plane constraint is affected by the specimen dimension parallel to the crack front, and the in-plane constraint is affected by the specimen dimension in the direction of crack propagation. The loss of constraint, such as the decreasing of crack depth, will result in the increasing of the fracture resistance.[2] That is to say, different specimens and structures with different crack sizes have different constraints and fracture behaviours.

In current structure integrity assessment standards, the standard specimens have severely size requirements to ensure the highest constraint and the lowest fracture resistance.[3–8] Moreover, the obtained fracture resistance data of the standard specimen by fracture mechanics test were selected to evaluate the safety of

[1]Shanghai Key Laboratory of Multiphase Flow and Heat Transfer in Power Engineering, School of Energy and Power Engineering, University of Shanghai for Science and Technology, Shanghai, China
[2]Department of Mechanical & Aerospace Engineering, University of Strathclyde, Glasgow, UK

Corresponding author:
Jie Yang, Shanghai Key Laboratory of Multiphase Flow and Heat Transfer in Power Engineering, School of Energy and Power Engineering, University of Shanghai for Science and Technology, Shanghai 200093, China.
Email: yangjie@usst.edu.cn

the structure. However, for the structures with lower constraints than standard specimen, the transfer of fracture resistance data from standard specimen to the actual cracked structures will produce a conservative result. Conversely, for some special structures with higher constraints than standard specimen, the transfer will result in a non-conservative result. Thus, for accurate structure integrity assessment, the constraint matching specimen (may not be the standard specimen) should be selected to assess the safety of the actual cracked structure, and the matching of constraint between laboratory specimens and actual cracked structures becomes the key problem of the structure integrity assessment.

To address this problem, several constraint parameters were established to quantify the constraint state, which contains the out-of-plane constraint parameter T_Z[9–11] and the in-plane constraint parameters T,[12] Q[13,14] and A_2.[15] These parameters have been used successfully to quantify the out-of-plane or in-plane constraint separately. Unfortunately, both out-of-plane and in-plane constraints generally existing in the actual structures, these parameters above cannot be used to establish the matching of constraint between laboratory specimens and actual structures.

Some unified parameters, such as φ[16,17] and A_p,[18,19] which can quantify both out-of-plane and in-plane constraints were further established. Compared with the constraint parameter φ, the unified parameter A_p can be used in the steel with higher toughness.[20] And with development of these unified constraint parameters, the matching of constraint can be researched in a brand-new angle of view.

In the previous studies, based on the unified constraint parameter A_p, the authors studied the matching of constraint between standard specimen and non-standard specimens,[21] between different laboratory specimens,[22] between cracked pipe structures and different laboratory specimens.[23] But for the steam turbine blade which is the core component of the steam turbine,[24] the constraint state is not clear yet, and the matching of constraint between the steam turbine blades and laboratory specimens has not been established. Thus, in this article, the constraints of cracked steam turbine blades were calculated, and the matching of constraint between the steam turbine blades and laboratory specimens was investigated.

Finite element calculation

Materials

To ensure the consistency with previous studies, the steel A508 was also selected. Its elastic modulus, Poisson's ratio and yield strength at room temperature are 202,410 MPa, 0.3 and 514 MPa, respectively. The true stress–strain curve of the A508 steel was shown in Figure 1.[25]

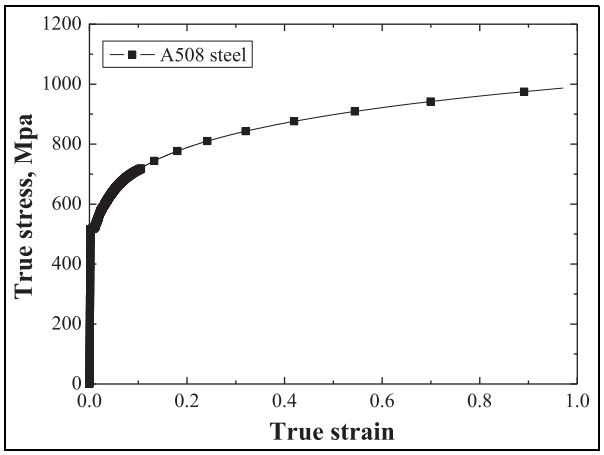

Figure 1. The true stress–strain curve of A508 steel.[25]

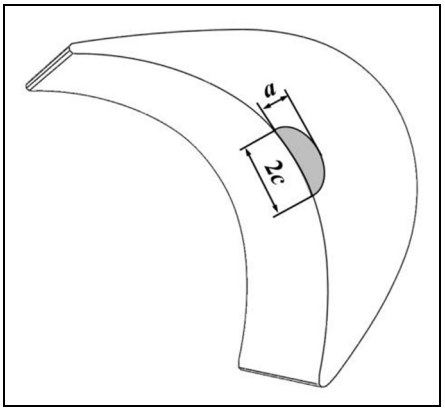

Figure 2. The geometry of the steam turbine blade with initial crack.

The geometries of the steam turbine blades

The governing-stage moving blade which used in the steam turbine was selected in this study, it is also the core component of the steam turbine. To obtain the constraints of the cracked steam turbine blades, an imaginary initial crack with different crack lengths and crack depths was set near the pressure side and the junction with the blade root, as shown in Figure 2. When the crack depth a was changed, fixing the crack length $2c = 50$ mm, and changing the $a/2c = 0.15$, 0.20, 0.25, 0.30, 0.35 and 0.45; when the crack length $2c$ was changed, fixing the crack depth $a = 15$ mm, and changing the $a/2c = 0.30$, 0.40 and 0.50.

The geometries of different laboratory specimens

To obtain the constraints of different laboratory specimens, the compact tension (CT), single edge-notched bend (SENB), single edge-notched tensile (SENT) and central-cracked tension (CCT) specimens were selected, and seven values of crack depths denoted as $a/W = 0.1$, 0.2, 0.3, 0.4, 0.5, 0.6 and 0.7 were set for each specimen.

Table 1. The sizes of different laboratory specimens.

Specimen	*L* (mm)	*W* (mm)	*a* (mm)	*a*/*W*	*B*/*W*
SENB	128	32	3.2	0.1	Plane strain
SENB	128	32	6.4	0.2	Plane strain
SENB	128	32	9.6	0.3	Plane strain
SENB	128	32	12.8	0.4	Plane strain
SENB	128	32	16	0.5	Plane strain
SENB	128	32	19.2	0.6	Plane strain
SENB	128	32	22.4	0.7	Plane strain
CT, SENT and CCT		32	3.2	0.1	Plane strain
CT, SENT and CCT		32	6.4	0.2	Plane strain
CT, SENT and CCT		32	9.6	0.3	Plane strain
CT, SENT and CCT		32	12.8	0.4	Plane strain
CT, SENT and CCT		32	16	0.5	Plane strain
CT, SENT and CCT		32	19.2	0.6	Plane strain
CT, SENT and CCT		32	22.4	0.7	Plane strain

SENB: single edge-notched bend; CT: compact tension; SENT: single edge-notched tensile; CCT: central-cracked tension.

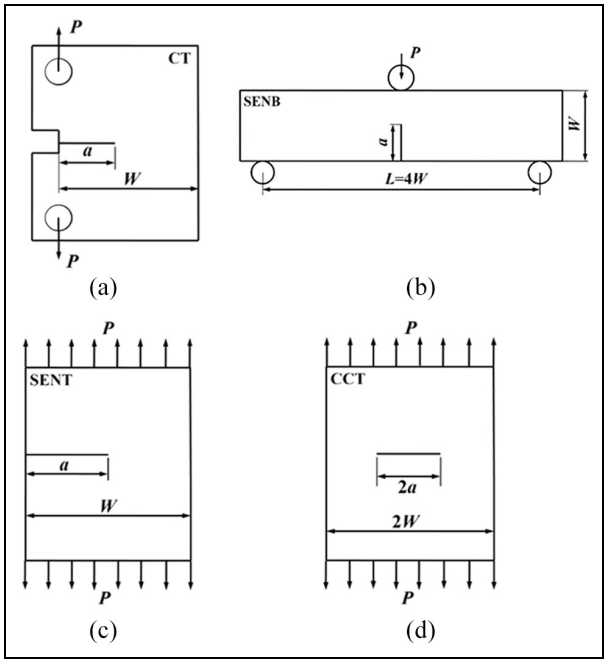

Figure 3. The geometries of different laboratory specimens: (a) SENB, (b) CT, (c) SENT and (d) CCT.

The geometries and sizes of different laboratory specimens were shown in Figure 3 and Table 1.

Finite element model

The commercial finite element code ABAQUS was used in this study. In addition, the two-dimensional (2D) plane strain 8-node solid element with reduced integration (CPE8R) was used for different laboratory specimens, and the three-dimensional (3D) 8-node brick element with reduced integration (C3D8R) was used for the steam turbine blades. A fine mesh configuration which has a focused ring of elements surrounding the crack front was used in all the specimens and blades.[18,19] The finite element model of typical steam turbine blade was shown in Figure 4, it contains 49,039 nodes and 44,865 elements.

Furthermore, for the SENB specimens, the load was applied at the up centre of the specimen by prescribing a displacement of 6 mm; for the CT specimens, the load was applied at the centre of the loading hole by applying a concentrated load; for the SENT and CCT specimens, the load was applied by applying a uniform load. For the blade, the internal pressure was 15.2184 MPa and the bending moment was applied on the back of the steam turbine blade for loading.

And then, the parameter A_p which defined as

$$A_p = \frac{A_{PEEQ}}{A_{ref}} \tag{1}$$

was calculated, where A_{PEEQ} is the area surrounded by the equivalent plastic strain isoline at crack tip and A_{ref} is the reference area surrounded by the equivalent plastic strain isoline in a standard test at fracture.[18,19] In addition, the J/J_{ref}-$\sqrt{A_p}$ lines were established.

Because the slope of the $J/J_{ref}-\sqrt{A_p}$ line reflects the constraint of a specimen or structure, if two $J/J_{ref}-\sqrt{A_p}$ lines are coincide, their constraints are matching.[21] Thus, this study was focusing on the $J/J_{ref}-\sqrt{A_p}$ lines and their slopes of different steam turbine blades and laboratory specimens.

Results and discussion

The matching of constraint between steam turbine blades and SENB specimens

The comparisons of $J/J_{ref}-\sqrt{A_p}$ lines between steam turbine blades and SENB specimens were shown in Figure 5.

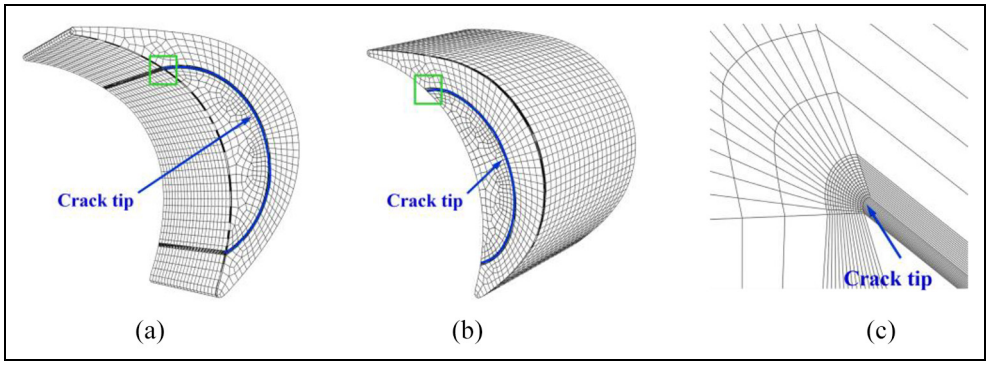

Figure 4. The mesh partition of the typical steam turbine blade model: (a) the front, (b) the back and (c) the local meshes of the square location in the (a) and (b).

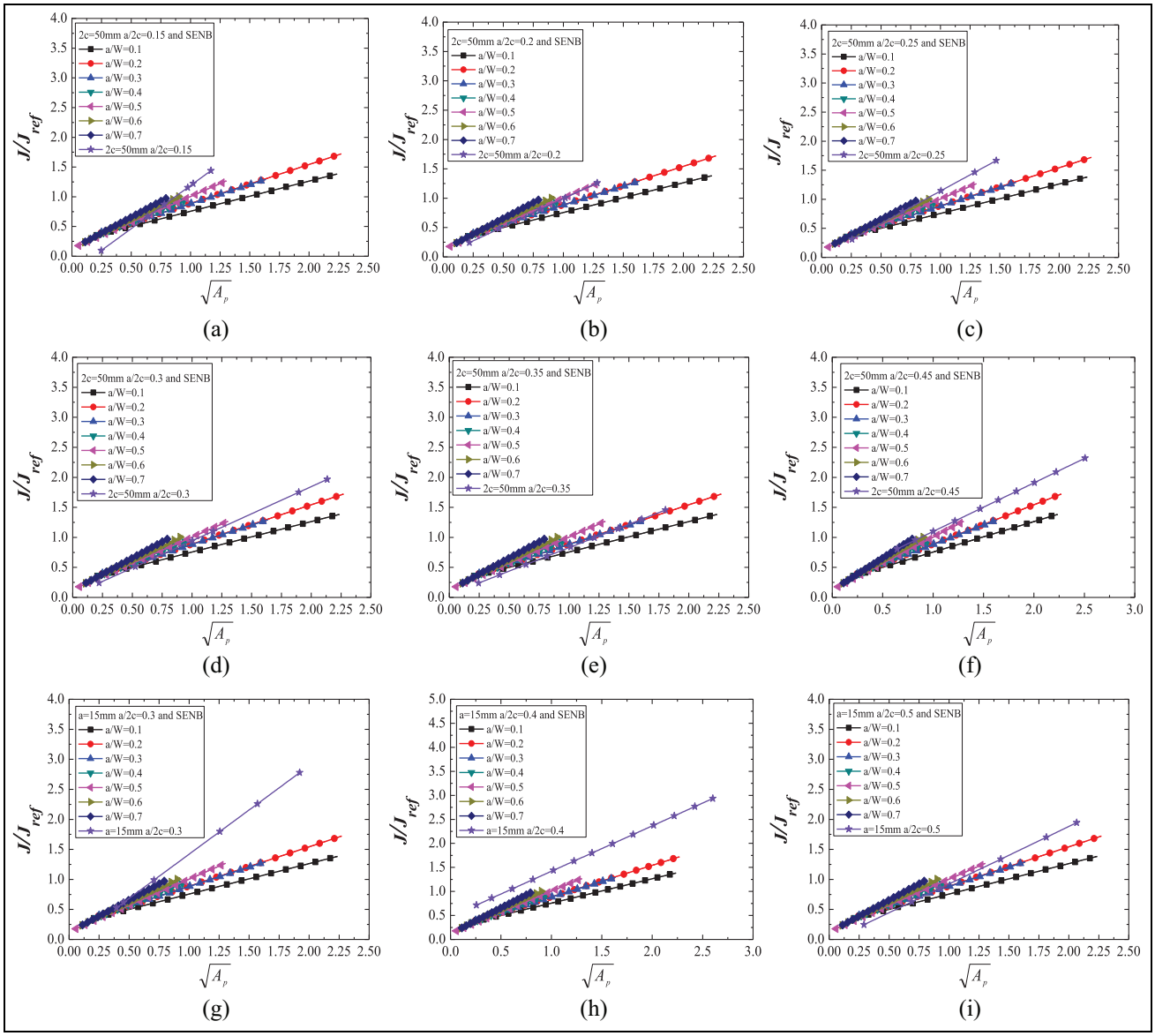

Figure 5. The matching of constraints between steam turbine blades and SENB specimens: (a) the blade with $2c = 50$, $a/2c = 0.15$ and SENB; (b) the blade with $2c = 50$, $a/2c = 0.20$ and SENB; (c) the blade with $2c = 50$, $a/2c = 0.25$ and SENB; (d) the blade with $2c = 50$, $a/2c = 0.30$ and SENB; (e) the blade with $2c = 50$, $a/2c = 0.35$ and SENB; (f) the blade with $2c = 50$, $a/2c = 0.45$ and SENB; (g) the blade with $a = 15$, $a/2c = 0.30$ and SENB; (h) the blade with $a = 15$, $a/2c = 0.40$ and SENB; and (i) the blade with $a = 15$, $a/2c = 0.50$ and SENB.

Table 2. The values of a and b for the mathematical expressions of the SENB specimens and steam turbine blades.

SENB	a	b	Blade	a	b
$a/W = 0.1$	0.51	0.25	$2c = 50$ mm, $a/2c = 0.15$	1.45	–0.26
$a/W = 0.2$	0.66	0.23	$2c = 50$ mm, $a/2c = 0.20$	0.96	0.03
$a/W = 0.3$	0.64	0.24	$2c = 50$ mm, $a/2c = 0.25$	1.12	0.02
$a/W = 0.4$	0.79	0.19	$2c = 50$ mm, $a/2c = 0.30$	0.90	0.04
$a/W = 0.5$	0.87	0.13	$2c = 50$ mm, $a/2c = 0.35$	0.78	0.05
$a/W = 0.6$	0.97	0.13	$2c = 50$ mm, $a/2c = 0.45$	0.81	0.29
$a/W = 0.7$	1.08	0.12	$a = 15$ mm, $a/2c = 0.30$	1.47	–0.05
			$a = 15$ mm, $a/2c = 0.40$	0.95	0.47
			$a = 15$ mm, $a/2c = 0.50$	0.96	–0.03

SENB: single edge-notched bend.

Table 3. The values of a and b for the mathematical expressions of the CT specimens and steam turbine blades.

CT	a	b	Blade	a	b
$a/W = 0.1$	0.45	0.16	$2c = 50$ mm, $a/2c = 0.15$	1.45	–0.26
$a/W = 0.2$	0.51	0.24	$2c = 50$ mm, $a/2c = 0.20$	0.96	0.03
$a/W = 0.3$	0.60	0.25	$2c = 50$ mm, $a/2c = 0.25$	1.12	0.02
$a/W = 0.4$	1.10	0.28	$2c = 50$ mm, $a/2c = 0.30$	0.90	0.04
$a/W = 0.5$	1.36	0.14	$2c = 50$ mm, $a/2c = 0.35$	0.78	0.05
$a/W = 0.6$	1.36	0.18	$2c = 50$ mm, $a/2c = 0.45$	0.81	0.29
$a/W = 0.7$	1.39	0.17	$a = 15$ mm, $a/2c = 0.30$	1.47	–0.05
			$a = 15$ mm, $a/2c = 0.40$	0.95	0.47
			$a = 15$ mm, $a/2c = 0.50$	0.96	–0.03

CT: compact tension.

It can be found that for the SENB specimens, with increasing of the a/W, the slopes of the $J/J_{ref}-\sqrt{A_p}$ lines increase, which means that the $J/J_{ref}-\sqrt{A_p}$ lines reflect the right law, the constraints of SENB specimens increase with increasing of the crack depth.

In addition, the $J/J_{ref}-\sqrt{A_p}$ lines of some steam turbine blades are coincide with the SENB specimens, but not all the steam turbine blades can find an accordant SENB specimen to match the constraint. That is, if only the SENB standard specimen or only one specimen was selected to assess the structure integrity of the steam turbine blade, the inaccurate assessment results may be obtained. All the $J/J_{ref}-\sqrt{A_p}$ lines can be expressed in the form of $y = ax + b$, and the values of a and b were listed in Table 2.

Combined with mathematical expressions, and compared with the $J/J_{ref}-\sqrt{A_p}$ lines between steam turbine blades and SENB specimens, it can be found that the constraint of the steam turbine blade with $2c = 50$ mm, $a/2c = 0.20$ is similar to the SENB specimen with $a/W = 0.6$. The constraint of the steam turbine blade with $2c = 50$ mm, $a/2c = 0.25$ is similar to the SENB specimen with $a/W = 0.7$. The constraint of the steam turbine blade with $2c = 50$ mm, $a/2c = 0.30$ is similar to the SENB specimen with $a/W = 0.5$. The constraint of the steam turbine blade with $2c = 50$ mm, $a/2c = 0.35$ is similar to the SENB specimen with $a/W = 0.4$. The constraint of the steam turbine blade with $a = 15$ mm, $a/2c = 0.50$ is similar to the SENB specimen with $a/W = 0.5$.

The matching of constraint between steam turbine blades and CT specimens

The comparisons of $J/J_{ref}-\sqrt{A_p}$ lines between steam turbine blades and CT specimens were shown in Figure 6, and the mathematical expressions of the $J/J_{ref}-\sqrt{A_p}$ lines of all the steam turbine blades and CT specimens were shown in Table 3.

Compared with the $J/J_{ref}-\sqrt{A_p}$ lines between steam turbine blades and CT specimens, it can be found that the constraint of the steam turbine blade with $2c = 50$ mm, $a/2c = 0.35$ is similar to the CT specimen with $a/W = 0.3$. The constraint of the steam turbine blade with $a = 15$ mm, $a/2c = 0.30$ is similar to the CT specimen with $a/W = 0.7$. The constraint of the steam turbine blade with $a = 15$ mm, $a/2c = 0.40$ is similar to the CT specimen with $a/W = 0.4$.

Because the CT specimen is another standard specimen, the matching conditions between steam turbine blades and CT specimens also shows that it is not appropriate if only the standard specimen was selected

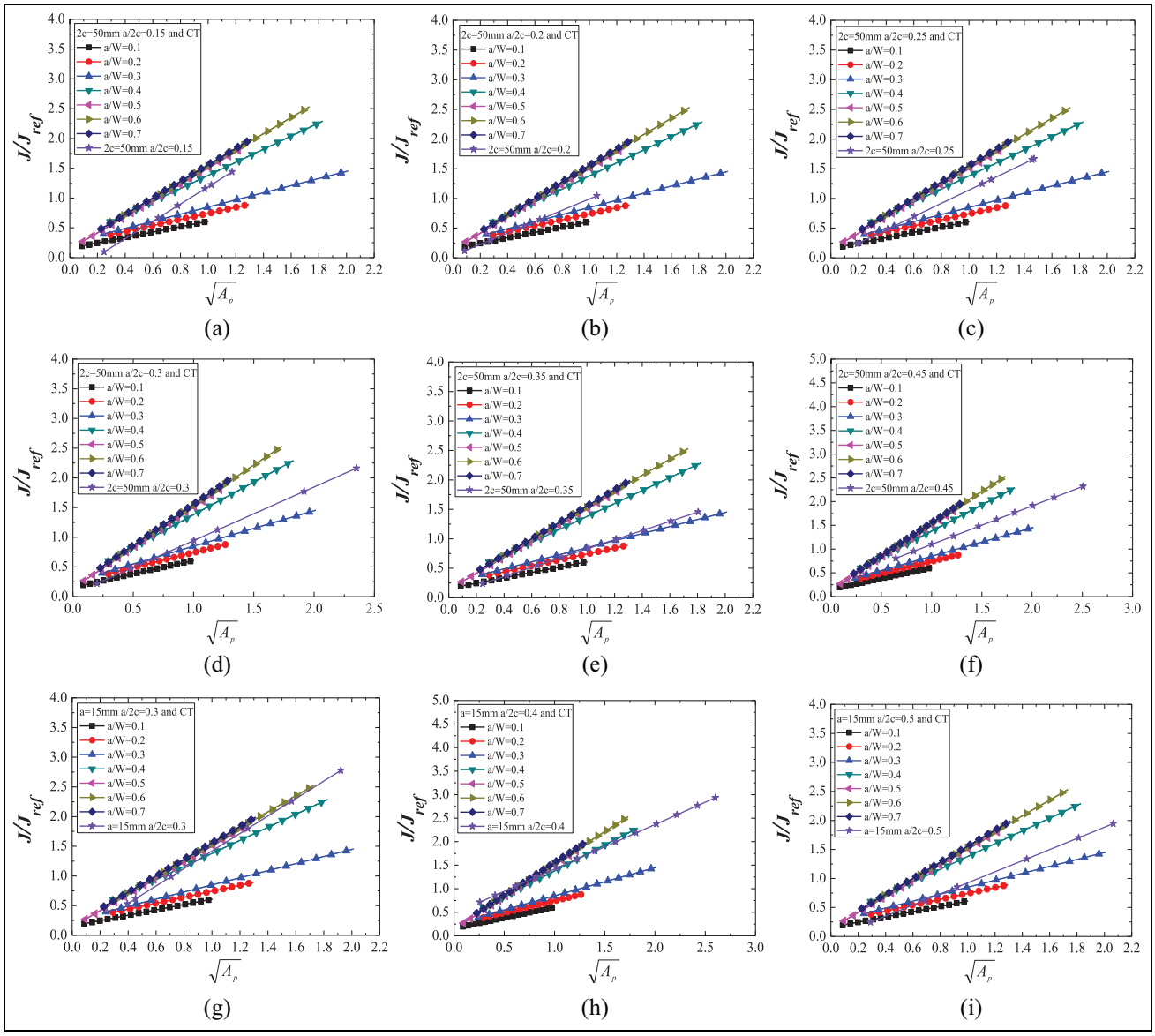

Figure 6. The matching of constraints between steam turbine blades and CT specimens: (a) the blade with $2c = 50$, $a/2c = 0.15$ and CT; (b) the blade with $2c = 50$, $a/2c = 0.20$ and CT; (c) the blade with $2c = 50$, $a/2c = 0.25$ and CT; (d) the blade with $2c = 50$, $a/2c = 0.30$ and CT; (e) the blade with $2c = 50$, $a/2c = 0.35$ and CT; (f) the blade with $2c = 50$, $a/2c = 0.45$ and CT; (g) the blade with $a = 15$, $a/2c = 0.30$ and CT; (h) the blade with $a = 15$, $a/2c = 0.40$ and CT; and (i) the blade with $a = 15$, $a/2c = 0.50$ and CT.

in the structure integrity assessment. Compared with the SENB specimens, the constraints of CT specimens reflect the same change rule, but have a much wider range.

The matching of constraint between steam turbine blades and SENT specimens

The comparisons of $J/J_{ref}-\sqrt{A_p}$ lines between steam turbine blades and SENT specimens were shown in Figure 7, and the mathematical expressions of the $J/J_{ref}-\sqrt{A_p}$ lines of all the steam turbine blades and SENT specimens were shown in Table 4.

Compared with the $J/J_{ref}-\sqrt{A_p}$ lines between steam turbine blades and SENT specimens, it can be found that the constraint of the steam turbine blade with $2c = 50\,\text{mm}$, $a/2c = 0.20$ is similar to the SENT specimen with $a/W = 0.3$. The constraint of the steam turbine blade with $2c = 50\,\text{mm}$, $a/2c = 0.30$ is similar to the SENT specimen with $a/W = 0.1$. The constraint of the steam turbine blade with $a = 15\,\text{mm}$, $a/2c = 0.30$ is similar to the SENT specimen with $a/W = 0.5$.

The constraints of the SENT specimens in this study is high, it is related to the loading mode. The constraints of the SENT specimens under different loading modes have been discussed in the previous study.[22]

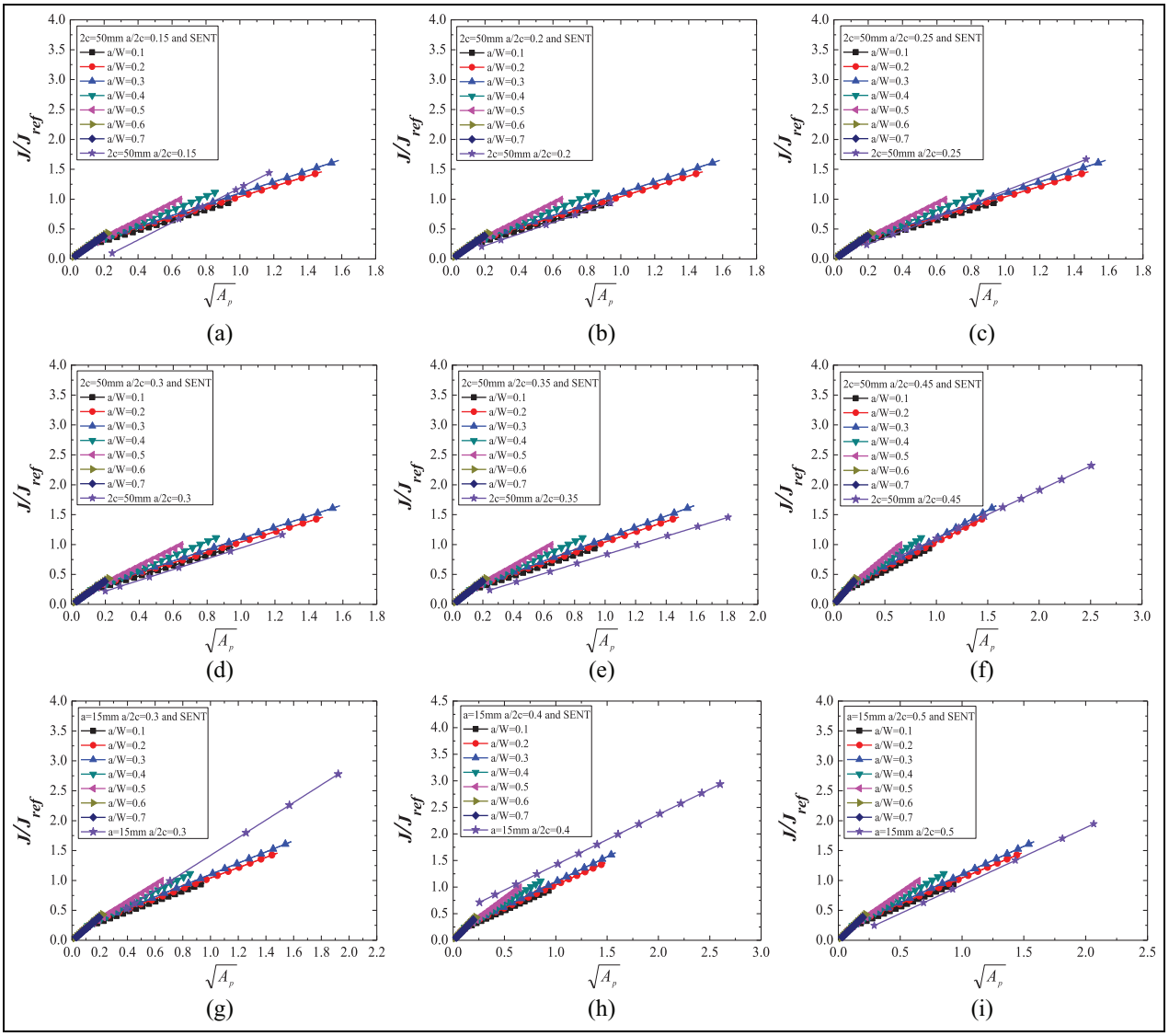

Figure 7. The matching of constraints between steam turbine blades and SENT specimens: (a) the blade with $2c = 50$, $a/2c = 0.15$ and SENT; (b) the blade with $2c = 50$, $a/2c = 0.20$ and SENT; (c) the blade with $2c = 50$, $a/2c = 0.25$ and SENT; (d) the blade with $2c = 50$, $a/2c = 0.30$ and SENT; (e) the blade with $2c = 50$, $a/2c = 0.35$ and SENT; (f) the blade with $2c = 50$, $a/2c = 0.45$ and SENT; (g) the blade with $a = 15$, $a/2c = 0.30$ and SENT; (h) the blade with $a = 15$, $a/2c = 0.40$ and SENT; and (i) the blade with $a = 15$, $a/2c = 0.50$ and SENT.

Table 4. The values of a and b for the mathematical expressions of the SENT specimens and steam turbine blades.

SENT	a	b	Blade	a	b
$a/W = 0.1$	0.87	0.13	$2c = 50$ mm, $a/2c = 0.15$	1.45	–0.26
$a/W = 0.2$	0.87	0.18	$2c = 50$ mm, $a/2c = 0.20$	0.96	0.03
$a/W = 0.3$	0.94	0.16	$2c = 50$ mm, $a/2c = 0.25$	1.12	0.02
$a/W = 0.4$	1.18	0.10	$2c = 50$ mm, $a/2c = 0.30$	0.90	0.04
$a/W = 0.5$	1.42	0.07	$2c = 50$ mm, $a/2c = 0.35$	0.78	0.05
$a/W = 0.6$	2.00	–0.01	$2c = 50$ mm, $a/2c = 0.45$	0.81	0.29
$a/W = 0.7$	2.00	–0.01	$a = 15$ mm, $a/2c = 0.30$	1.47	–0.05
			$a = 15$ mm, $a/2c = 0.40$	0.95	0.47
			$a = 15$ mm, $a/2c = 0.50$	0.96	–0.03

SENT: single edge-notched tensile.

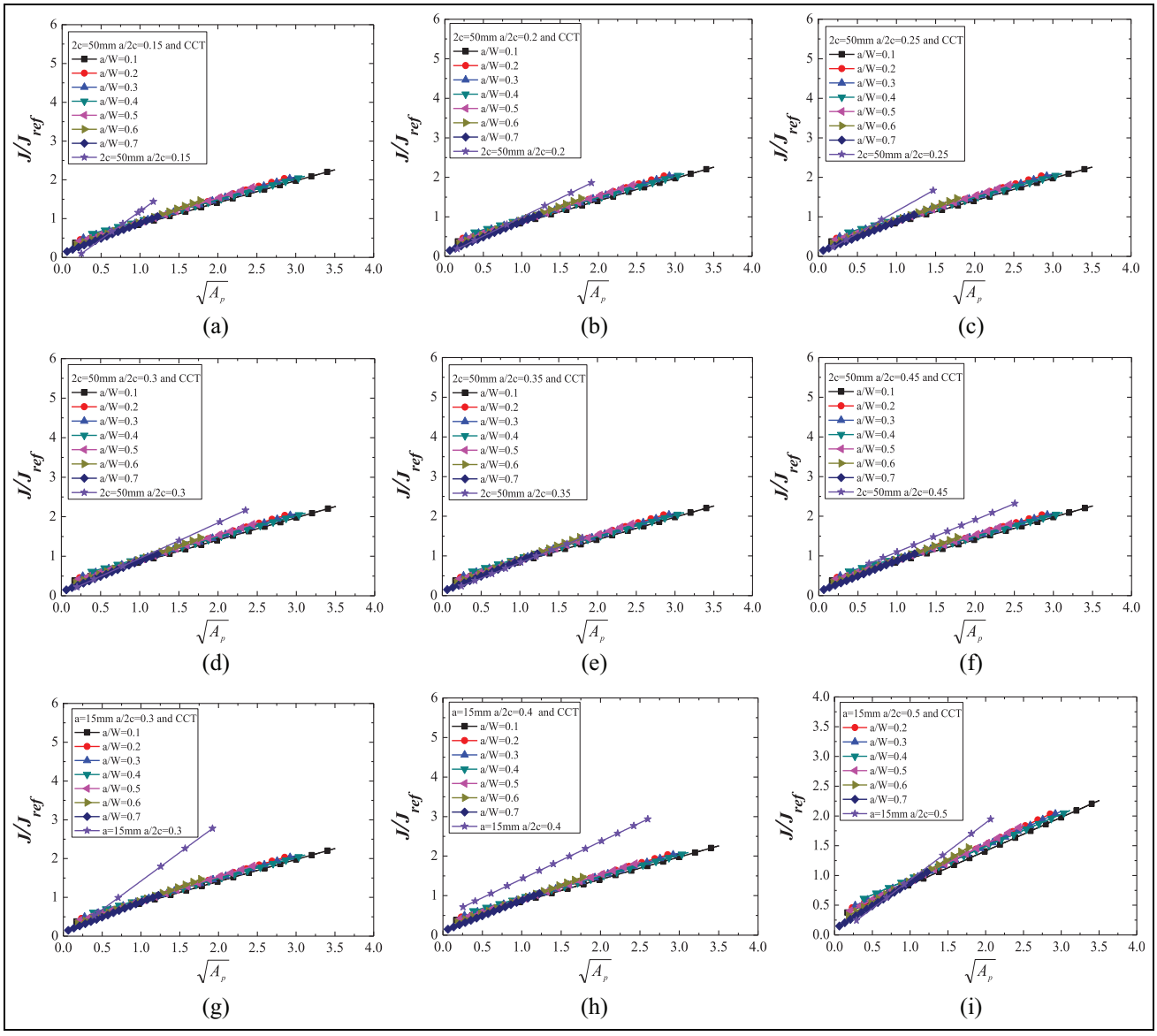

Figure 8. The matching of constraints between steam turbine blades and CCT specimens: (a) the blade with $2c = 50$, $a/2c = 0.15$ and CCT; (b) the blade with $2c = 50$, $a/2c = 0.20$ and CCT; (c) the blade with $2c = 50$, $a/2c = 0.25$ and CCT; (d) the blade with $2c = 50$, $a/2c = 0.30$ and CCT; (e) the blade with $2c = 50$, $a/2c = 0.35$ and CCT; (f) the blade with $2c = 50$, $a/2c = 0.45$ and CCT; (g) the blade with $a = 15$, $a/2c = 0.30$ and CCT; (h) the blade with $a = 15$, $a/2c = 0.40$ and CCT; and (i) the blade with $a = 15$, $a/2c = 0.50$ and CCT.

The matching of constraint between steam turbine blades and CCT specimens

The comparisons of $J/J_{ref} - \sqrt{A_p}$ lines between steam turbine blades and CCT specimens were shown in Figure 8, and the mathematical expressions of the $J/J_{ref} - \sqrt{A_p}$ lines of all the steam turbine blades and CCT specimens were shown in Table 5.

Compared with the $J/J_{ref} - \sqrt{A_p}$ lines between steam turbine blades and CCT specimens, it can be found that the matching of constraint between blades and CCT specimens is poor, only the constraint of the steam turbine blade with $2c = 50\,\text{mm}$, $a/2c = 0.35$ is similar to the CCT specimen with $a/W = 0.7$. Thus, for the steam turbine blades, the CCT specimen is not an appropriate specimen to be selected in the structure integrity assessment. Compared with the other three kinds of specimens, the constraints of CCT specimens with different crack depths are similar and have a much narrower range of constraint.

The results above show that the constraint matching laboratory specimen with the steam turbine blade can be found in this way, but the matching specimen not always the standard specimen. For the fracture behaviours of the constraint matching specimen and structure can be transferred each other, the constraint

Table 5. The values of a and b for the mathematical expressions of the CCT specimens and steam turbine blades.

CCT	a	b	Blade	a	b
$a/W = 0.1$	0.56	0.28	$2c = 50$ mm, $a/2c = 0.15$	1.45	–0.26
$a/W = 0.2$	0.60	0.32	$2c = 50$ mm, $a/2c = 0.20$	0.96	0.03
$a/W = 0.3$	0.58	0.33	$2c = 50$ mm, $a/2c = 0.25$	1.12	0.02
$a/W = 0.4$	0.54	0.40	$2c = 50$ mm, $a/2c = 0.30$	0.90	0.04
$a/W = 0.5$	0.63	0.28	$2c = 50$ mm, $a/2c = 0.35$	0.78	0.05
$a/W = 0.6$	0.72	0.19	$2c = 50$ mm, $a/2c = 0.45$	0.81	0.29
$a/W = 0.7$	0.78	0.10	$a = 15$ mm, $a/2c = 0.30$	1.47	–0.05
			$a = 15$ mm, $a/2c = 0.40$	0.95	0.47
			$a = 15$ mm, $a/2c = 0.50$	0.96	–0.03

CCT: central-cracked tension.

Table 6. The summary of the constraint matching between steam turbine blades and laboratory specimens.

	Blade 1	Blade 2	Blade 3	Blade 4	Blade 5	Blade 6	Blade 7	Blade 8	Blade 9
SENB $a/W = 0.1$									
SENB $a/W = 0.2$									
SENB $a/W = 0.3$									
SENB $a/W = 0.4$					Yes				
SENB $a/W = 0.5$				Yes					Yes
SENB $a/W = 0.6$		Yes							
SENB $a/W = 0.7$			Yes						
CT $a/W = 0.1$									
CT $a/W = 0.2$									
CT $a/W = 0.3$					Yes				
CT $a/W = 0.4$								Yes	
CT $a/W = 0.5$									
CT $a/W = 0.6$									
CT $a/W = 0.7$							Yes		
SENT $a/W = 0.1$				Yes					
SENT $a/W = 0.2$									
SENT $a/W = 0.3$		Yes							
SENT $a/W = 0.4$									
SENT $a/W = 0.5$							Yes		
SENT $a/W = 0.6$									
SENT $a/W = 0.7$									
CCT $a/W = 0.1$									
CCT $a/W = 0.2$									
CCT $a/W = 0.3$									
CCT $a/W = 0.4$									
CCT $a/W = 0.5$									
CCT $a/W = 0.6$									
CCT $a/W = 0.7$					Yes				

SENB: single edge-notched bend; CT: compact tension; SENT: single edge-notched tensile; CCT: central-cracked tension.

matching specimen should be found and selected first in the structure integrity assessment. And then, the tested mechanics properties of the constraint matching specimen can be used in the assessment to improve the accurately of the assessment.

Generally, the defect sizes can be measured by non-destructive testing. And then, based on the relevant standards, the defects in the structure were usually merged and characterized by a semi-elliptical or elliptical crack. The parameters 'a' and 'c' of the blade can be determined in this way. This is also the reason for the selection of the semi-elliptical crack in this study. Actually, in the assessment of the steam turbine blade, the parameters 'a' and 'c' of the blade are not always needed to be determined. When the crack size was measured by non-destructive testing, the finite element model of the blade with the actual crack can be built to calculate the computed line. And then, based on the methods in this article, different specimens can be calculated to try to find an accurate constraint matching specimen with the cracked blade.

The summary of the constraint matching between steam turbine blades and laboratory specimens

In order to descript the results in a concise and clear way, the steam turbine blades with $2c = 50\,\text{mm}$, $a/2c = 0.15$; $2c = 50\,\text{mm}$, $a/2c = 0.20$; $2c = 50\,\text{mm}$, $a/2c = 0.25$; $2c = 50\,\text{mm}$, $a/2c = 0.30$; $2c = 50\,\text{mm}$, $a/2c = 0.35$; $2c = 50\,\text{mm}$, $a/2c = 0.45$; $a = 15\,\text{mm}$, $a/2c = 0.30$; $a = 15\,\text{mm}$, $a/2c = 0.40$; and $a = 15\,\text{mm}$, $a/2c = 0.50$ were marked as blade 1, blade 2, blade 3, blade 4, blade 5, blade 6, blade 7, blade 8 and blade 9, respectively.

The summary of the constraint matching between steam turbine blades and different laboratory specimens were shown in Table 6. If the constraints of the specimen and the blade were matching, marking as yes in Table 6. If the constraints of the specimen and the blade were un-matching, nothing is marked in Table 6.

Conclusion

1. The matching of constraint between steam turbine blade and different laboratory specimens has been established.
2. The constraints of the steam turbine blades with different crack sizes were quite different, if only the standard specimen or only one specimen was selected to assess the structure integrity of the blades, the inaccurate assessment results will be obtained.
3. In the structure integrity assessment, a specimen with similar constraint to the blade can be selected for the mechanics test, and the tested mechanics properties can be used in the assessment to improve the accurately of the assessment.
4. The CCT specimens need to be avoided for selecting in the assessment of the steam turbine blades.

Declaration of conflicting interests

The author(s) declared no potential conflicts of interest with respect to the research, authorship and/or publication of this article.

Funding

The author(s) disclosed receipt of the following financial support for the research, authorship and/or publication of this article: This research was funded by National Natural Science Foundation of China, grant numbers 51975378 and 51605292.

ORCID iD

Jie Yang https://orcid.org/0000-0001-6906-9012

Supplemental Material

Supplemental material for this article is available online.

References

1. Brocks W and Schmitt W. The second parameter in J-R curves: constraint or triaxiality. In: *2nd symposium on constraint effects*, Dallas, TX, 17–18 November 1993. Philadelphia, PA: ASTM International.
2. Dodds RH, Shih CF and Anderson TL. Continuum and micromechanics treatment of constraint in fracture. *Int J Fracture* 1993; 64: 101–133.
3. Qian GA, Cao YP, Niffenegger M, et al. Comparison of constraint analyses with global and local approaches under uniaxial and biaxial loadings. *Eur J Mech A: Solid* 2018; 69: 135–146.
4. Qian GA and Lei WS. A statistical model of fatigue failure incorporating effects of specimen size and load amplitude on fatigue life. *Philos Mag* 2019; 99: 2089–2125.
5. Liao D, Zhu SP and Qian GA. Multiaxial fatigue analysis of notched components using combined critical plane and critical distance approach. *Int J Mech Sci* 2019; 160: 38–50.
6. Liao D and Zhu SP. Energy field intensity approach for notch fatigue analysis. *Int J Fatigue* 2019; 127: 190–202.
7. Qian GA, Jian ZM, Pan XN, et al. In-situ investigation on fatigue behaviors of Ti-6Al-4V manufactured by selective laser melting. *Int J Fatigue* 2020; 133: 105424.
8. Zhang YC, Lu MJ, Jiang WC, et al. Effect of the geometrical size on time dependent failure probability of the solid oxide fuel cell. *Int J Hydrogen Energ* 2019; 44: 11033–11046.
9. Guo W. Elastoplastic three dimensional crack border field-I: singular structure of the field. *Eng Fract Mech* 1993; 46: 93–104.
10. Guo W. Elastoplastic three dimensional crack border field-II: asymptotic solution for the field. *Eng Fract Mech* 1993; 46: 105–113.
11. Guo W. Elastoplastic three dimensional crack border field-III: fracture parameters. *Eng Fract Mech* 1995; 51: 51–71.
12. Betegón C and Hancock JW. Two-parameter characterization of elastic-plastic crack-tip fields. *J Appl Mech* 1991; 58: 104–110.
13. O'Dowd NP and Shih CF. Family of crack-tip fields characterized by a triaxiality parameter-I: structure of fields. *J Mech Phys Solids* 1991; 39: 989–1015.
14. O'Dowd NP and Shih CF. Family of crack-tip fields characterized by a triaxiality parameter-II: fracture applications. *J Mech Phys Solids* 1992; 40: 939–963.
15. Chao YJ, Yang S and Sutton MA. On the fracture of solids characterized by one or two parameters: theory and practice. *J Mech Phys Solids* 1994; 42: 629–647.
16. Mostafavi M, Smith DJ and Pavier MJ. Reduction of measured toughness due to out-of-plane constraint in ductile fracture of aluminium alloy specimens. *Fatigue Fract Eng M* 2010; 33: 724–739.
17. Mostafavi M, Smith DJ and Pavier MJ. Fracture of aluminium alloy 2024 under biaxial and triaxial loading. *Eng Fract Mech* 2011; 78: 1705–1716.
18. Yang J, Wang GZ, Xuan FZ, et al. Unified characterisation of in-plane and out-of-plane constraint based on

crack-tip equivalent plastic strain. *Fatigue Fract Eng M* 2013; 36: 504–514.
19. Yang J, Wang GZ, Xuan FZ, et al. Unified correlation of in-plane and out-of-plane constraints with fracture toughness. *Fatigue Fract Eng M* 2014; 37: 132–145.
20. Yang J, Wang GZ, Xuan FZ, et al. Unified correlation of in-plane and out-of-plane constraint with fracture resistance of a dissimilar metal welded joint. *Eng Fract Mech* 2014; 115: 296–307.
21. Yang J. The matching of crack-tip constraint between standard and non-standard specimen. *Adv Mech Eng* 2018; 10: 1–8.
22. Yang J, Liu YM and Wu F. Study on the matching of crack-tip constraints among different laboratory specimens. *J Mech Strength* 2019; 6: 1308–1314.
23. Yang J and Liu YM. Matching of crack-tip constraint between pipe structures and different laboratory specimens. *Mater Mech Eng* 2019; 43: 43–47.
24. Zhu XC, Chen HF, Xuan FZ, et al. On the creep fatigue and creep rupture behaviours of 9-12% Cr steam turbine rotor. *Eur J Mech A: Solid* 2019; 76: 263–278.
25. Wang HT, Wang GZ, Xuan FZ, et al. Numerical investigation of ductile crack growth behavior in a dissimilar metal welded joint. *Nucl Eng Des* 2011; 241: 3234–3243.